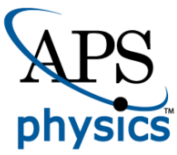

Systematic comparison of jet quenching in different fluid-dynamical models

Thorsten Renk, Hannu Holopainen, Ulrich Heinz, and Chun Shen

Phys. Rev. C **83**, 014910 — Published 28 January 2011

DOI: 10.1103/PhysRevC.83.014910

A systematic comparison of jet quenching in different fluid-dynamical models

Thorsten Renk* and Hannu Holopainen†
Department of Physics, P.O. Box 35, FI-40014 University of Jyväskylä, Finland and Helsinki Institute of Physics, P.O. Box 64, FI-00014 University of Helsinki, Finland

Ulrich Heinz‡ and Chun Shen§
Department of Physics, The Ohio State University, Columbus, OH 43210, USA
(Dated: December 16, 2010)

Comparing four different (ideal and viscous) hydrodynamic models for the evolution of the medium created in 200 A GeV Au-Au collisions, combined with two different models for the path length dependence of parton energy loss, we study the effects of jet quenching on the emission-angle dependence of the nuclear suppression factor $R_{AA}(\phi)$ and the away-side per trigger yield $I_{AA}(\phi)$. Each hydrodynamic model was tuned to provide a reasonable description of the single-particle transverse momentum spectra for all collision centralities, and the energy loss models were adjusted to yield the same pion nuclear suppression factor in central Au-Au collisions. We find that the experimentally measured in-plane vs. out-of-plane spread in $R_{AA}(\phi)$ is better reproduced by models that shift the weight of the parton energy loss to later times along its path. Among the models studied here, this is best achieved by energy loss models that suppress energy loss at early times, combined with hydrodynamic models that delay the dilution of the medium density due to hydrodynamic expansion by viscous heating. We were unable to identify a clear tomographic benefit of a measurement of $I_{AA}(\phi)$ over that of $R_{AA}(\phi)$.

PACS numbers: 25.75.-q,25.75.Gz

I. INTRODUCTION

The expression 'jet tomography' is often used to describe the analysis of hard pQCD processes taking place inside the soft medium created in an ultrarelativistic heavy-ion collision, with the aim to study properties of the medium. In particular, the focus is often on the nuclear suppression of hard hadrons in A-A collisions compared with the scaled expectation from p-p collisions, due to loss of energy from the hard parton by interactions with the soft medium (see e.g. [1–5]), expressed through the nuclear suppression factor R_{AA}.

In comparing theoretical calculations with experimental data on R_{AA}, there are two main unknown properties of the medium: The nature of the parton-medium interaction, being closely connected with microscopic properties of the medium (such as the relevant degrees of freedom), and the evolution of the medium density distribution, being connected with macroscopic properties such as the thermodynamical parameters in a fluid description of the medium. While some attempts at systematic comparison of different models for the parton-medium interactions using the same fluid-dynamical model for the medium have been made in order to assess the effect of assumptions in the parton-medium interaction model [6, 7], there is very little systematics available for the effect of different hydrodynamical models on jet quenching observables other than the overall suppression ratio $R_{AA}(p_T)$ [8, 9].

What may have slowed the insight that there is a need to systematically understand the role of the medium density evolution is the fact that early comparisons with data were usually done on the basis of single-hadron suppression R_{AA} for central collisions only, and it took some time before it was realized that this quantity is quite insensitive to model assumptions [10], especially when (as usually done) one model parameter governing the strength of the parton-medium interaction is fit to the data. The need for more differential observables, such as $R_{AA}(\phi)$ as a function of the angle of the observed hadron with the reaction plane for different centralities [11] or the strength suppression I_{AA} observed in hard back-to-back correlations [8], to overcome this insensitivity was only realized later.

Such observables are primarily sensitive to the effective path length dependence of the energy loss. As one goes from central to peripheral collisions, both the mean density of the medium and the average path length needed for a hard parton to traverse the medium decrease. Within a given centrality class, $R_{AA}(\phi)$ is dominated by the change in path length, modulated by a weak directional dependence of the average density probed by the parton. How precisely the path length and density change with centrality depends, however, on details of the hydrodynamical evolution.

The aim of this paper is to investigate in some detail the connection between high-p_T observables and the bulk medium evolution. In particular, we try to identify those properties of a hydrodynamical model which have the strongest influence on high-p_T observables. We

*Electronic address: thorsten.i.renk@jyu.fi
†Electronic address: hannu.l.holopainen@jyu.fi
‡Electronic address: heinz@mps.ohio-state.edu
§Electronic address: shen@mps.ohio-state.edu

do so by presenting a systematic study of the directional dependence of the nuclear suppression factor R_{AA} and the away-side yield in triggered back-to-back correlations, I_{AA}, for several parton-medium interaction models with different path length dependence and a number of different hydrodynamical models for the medium. The hope is to derive constraints for a combination of both medium evolution and parton-medium interaction models that can be used to eventually arrive at a detailed understanding of the dynamics of ultrarelativistic heavy-ion collisions.

II. HYDRODYNAMICAL MODELS

We describe the medium probed by the hard parton as a thermalized fluid. Its temperature and energy and particle densities evolve in space and time, due to hydrodynamic expansion driven by pressure gradients. In this work we use both ideal and viscous hydrodynamics to generate these density profiles.

A. Ideal hydrodynamics

In the ideal case we solve the hydrodynamic equations

$$\partial_\mu T^{\mu\nu} = 0, \quad \partial_\mu j_B^\mu = 0, \tag{1}$$

where $T^{\mu\nu} = (\epsilon + P)u^\mu u^\nu - g^{\mu\nu}P$ is the stress-energy tensor, $j_B^\mu = n_B u^\mu$ is the baryon number current, n_B is the net baryon number density, ϵ the energy density, and P the pressure in the local rest frame which moves with fluid four-velocity u^μ in the global frame. The Equation of State (EoS) $P = P(\epsilon, n_B)$, relating the pressure to the local energy and net baryon number density, closes the set of dynamical equations.

For testing parton energy loss, we have at our disposal space-time profiles of ϵ, P and temperature T from two different ideal hydrodynamical models. The first of these [12] solves Eqs. (1) in 3+1 dimensions, propagating both $T^{\mu\nu}$ and j_B^μ. The second model [13] simplifies the problem to 2+1 dimensions by assuming longitudinal boost invariance (i.e. none of the physical quantities depend on space-time rapidity $\eta = \frac{1}{2}\ln[(t+z)/(t-z)]$) and setting the net baryon density everywhere to zero (such that only the energy-momentum tensor $T^{\mu\nu}$ needs to be evolved, using a simplified form $P(\epsilon)$ for the EoS). These approximations can be made since we are interested in energy loss only at mid-rapidity where, at RHIC energies, the net baryon density is very small. Both calculations use light-cone coordinates (τ, x, y, η), where $\tau = \sqrt{t^2 - z^2}$ is the longitudinal proper time and η is the space-time rapidity.

Both models use smooth energy density distributions as initial conditions, based on the densities of binary collisions and wounded nucleons [14]. For details we refer to the original papers describing the models [12, 13]. The hydrodynamic evolution starts at initial time $\tau_0 = 0.6\ (0.17)\,\mathrm{fm}/c$ in the (3+1)-d ((2+1)-d) model. The (3+1)-d model uses a bag model EoS with a first order phase transition at $T_c = 160$ MeV [12] whereas the (2+1)-d model [13] uses the EoS from Ref. [15]. Both Equations of State assume chemical equilibrium among the hadrons in the dilute resonance gas phase below T_c. Thermal hadron spectra are calculated using the conventional Cooper-Frye method [16], where particle emission is calculated from a constant-temperature surface. The freeze-out temperature is $T_{\mathrm{dec}} = 130\ (160)\,\mathrm{MeV}$ for the (3+1)-d ((2+1)-d) model. Strong and electromagnetic two- and three-particle decays of unstable hadrons are taken into account before comparing with experimental data.

B. Viscous hydrodynamics

We also study parton energy loss in a medium whose space-time evolution is computed from viscous hydrodynamics, by solving the second-order Israel-Stewart equations in 2+1 dimensions as described in Ref. [17], assuming longitudinal boost invariance and zero net baryon density. Here the energy-momentum tensor of the fluid is decomposed as

$$T^{\mu\nu} = (\epsilon + P)u^\mu u^\nu - P g^{\mu\nu} + \pi^{\mu\nu} \tag{2}$$

which differs from the ideal fluid decomposition in Sec. II A by the appearance of the traceless and symmetric shear viscous pressure tensor $\pi^{\mu\nu}$ satisfying $u_\mu \pi^{\mu\nu} = 0$. Effects from bulk viscosity are neglected as small compared to $\pi^{\mu\nu}$ [18]. The energy-momentum conservation equations $\partial_\mu T^{\mu\nu} = 0$ are supplemented by the Israel-Stewart [19, 20] evolution equations for the viscous pressure components $\pi^{\mu\nu}$, see [17] for details.

The viscous hydrodynamic energy density profiles studied here were obtained with the Equation of State s95p-PCE described in [21] and Appendix C of Ref. [22]. It matches the latest lattice QCD data of the EoS at high temperatures with a chemically frozen hadron resonance gas EoS at low temperatures [21, 22] that uses non-equilibrium chemical potentials [23] to ensure preservation of the stable hadron ratios at their chemical freeze-out values as the system cools below the chemical decoupling temperature $T_{\mathrm{chem}} = 165\,\mathrm{MeV}$ that has been experimentally established [24].

In the viscous simulations we start the hydrodynamic evolution at $\tau_0 = 0.4\,\mathrm{fm}/c$ and decouple the hadron momentum spectra at $T_{\mathrm{dec}} = 130\,\mathrm{MeV}$. To compute the hadron spectra from the hydrodynamical output along the freeze-out surface we again use the Cooper-Frye prescription, but with a modified expression for the distribution function, $f(x,p) = f_{\mathrm{eq}}(x,p) + \delta f(x,p)$, where we add to the local equilibrium distribution a small viscous correction δf that depends on the viscous pressure components $\pi^{\mu\nu}(x)$ at freeze-out and grows quadratically with

p_T (see [17, 21] for details). The specific shear viscosity is fixed at $\eta/s = 0.2$, independent of temperature.

In addition to the Glauber model initial conditions used in the ideal fluid dynamical models, we also study a set of viscous hydrodynamic evolution models based on Color Glass (CGC-fKLN) initial conditions [25, 26] which, for noncentral collisions, feature somewhat larger initial eccentricities and surface density gradients than the Glauber model profiles (see Fig. 1 in [21] for a comparison of these profiles) and thus generate more radial and elliptic flow. We will label viscous hydrodynamic simulations initiated with Glauber model profiles as "vGlb", and those initiated with CGC-fKLN profiles as "vCGC". We will discuss the consequences of these differences on the directional dependence of energy loss suffered by a parton propagating through these fireballs.

Neither the ideal nor the viscous fluid simulations studied here account for event-by-event fluctuations of the initial shape and orientation of the collision fireball. Such calculations were recently reported both for ideal [27–29] and viscous hydrodynamics [30]. Source eccentricities and anisotropic flow are most strongly affected by these fluctuations at very small and very large impact parameters where the fireball is either almost round or very small. Neither of these two situations is of interest in our present study.

C. Spectra and elliptic flow from the hydrodynamic models

Whereas the directional dependence of the soft hadron spectra (i.e. their elliptic flow) reflects the momentum anisotropy of the hadron emitting source at freeze-out, the emission angle dependence of parton energy loss probes more directly the geometrical aspects of the fireball, i.e. its spatial deformation. Still, it may matter whether the hard parton moves with or against the collective flow as it propagates through the fireball, so the hydrodynamical models need to be tuned to give a reasonably accurate representation of the momentum-space structure of the fireball, as reflected in the final hadron spectra, before we test the influence of differences in their geometrical features on parton energy loss.

In this subsection we demonstrate that all models provide a reasonable description of the transverse momentum spectra of pions and protons over the entire range of collision centralities.[1] Testing the spectra for both a very light and a heavy hadron species, which react differently to radial collective flow [31], ensures that the appropriate amount of radial flow is generated in the evolution. The elliptic flow coefficient tests whether we also have the correct amount of flow anisotropy. Expressed in terms of velocity differences, the flow anisotropy is a small effect superimposed on a much larger radial flow velocity; while this anisotropy is crucial in determining the transport coefficients (in particular the shear viscosity) of the fireball fluid, it is not expected to lead to major modifications of the directional dependence of parton energy loss. It affects the latter mostly by influencing the evolution of the spatial deformation of the fireball. As we will see, the time dependences of the radius and shape of the fireball play minor roles in the parton energy loss; hence, it is not a serious problem for our analysis that the elliptic flow $v_2(p_T)$ is not well reproduced by some of the hydrodynamical models we have studied.

centrality	impact parameter	$\varepsilon_x^{\rm Gl}$	$\varepsilon_x^{\rm CGC}$
0-10%	3.16 fm	0.075	0.102
10-20%	5.78 fm	0.206	0.250
20-30%	7.49 fm	0.297	0.344
30-40%	8.87 fm	0.366	0.407
40-50%	10.1 fm	0.415	0.445
50-60%	11.1 fm	0.439	0.455

TABLE I: Centrality classes and the corresponding impact parameters and initial source eccentricities used in the hydrodynamical model.

Figure 1 shows the pion and proton spectra for 200 A GeV Au-Au collisions at various centralities, as obtained from the three different (2+1)-d hydrodynamical models. Tab. I shows the impact parameters we have evaluated for a given centrality class, based on a Glauber calculation. Except for the peripheral bins, the viscous simulations give slightly steeper pion p_T-distributions than the ideal fluid ones. This is a consequence of the different chemical composition in the hadronic phase as described in the preceding subsection [23, 34]. The proton spectra are markedly better described by viscous than by ideal hydrodynamics. Shear viscosity adds to the effective transverse pressure, generating more radial flow [17] and thus making the spectrum harder, as desired by the experimental data.[2] The somewhat steeper surface density gradients of the initial CGC energy density profile when compared to the Glauber model adds an additional

[1] Note that our goal is *not* to achieve a perfect description of the measured hadron spectra. It is unlikely [21] that such a description can be obtained within a purely hydrodynamic approach; a fully realistic dynamical model can not avoid describing the late hadronic freeze-out stage microscopically with kinetic theory [32, 33].

[2] In [21] it was shown that larger radial flow can also be generated by selecting lower freeze-out temperatures, with similar effects on pion and proton p_T-spectra (but *not* their elliptic flow) as caused by larger viscosity (which matters most at early times where the expansion rate is highest). This finding applies only, however, if an equation of state with a chemically frozen hadron gas stage (such as s95p-PCE [21, 22]) is used [34]; for chemically equilibrated equations of state, late radial flow makes not only the proton but also the pion spectrum harder which is inconsistent with the measured pion distribution.

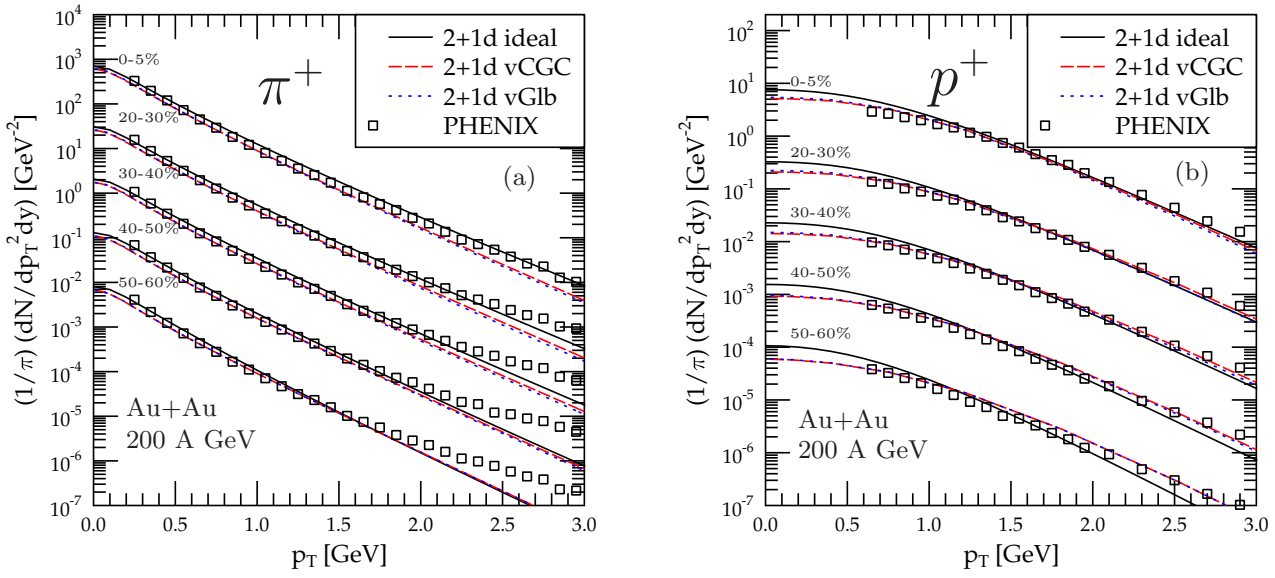

FIG. 1: (Color online) Transverse momentum spectra of positively charged pions (a) and protons (b) from ideal and viscous (2+1)-d models for 200 A GeV Au-Au collisions at different centralities. Data from the PHENIX Collaboration [39] are shown without error bars since errors are smaller than the symbol size.

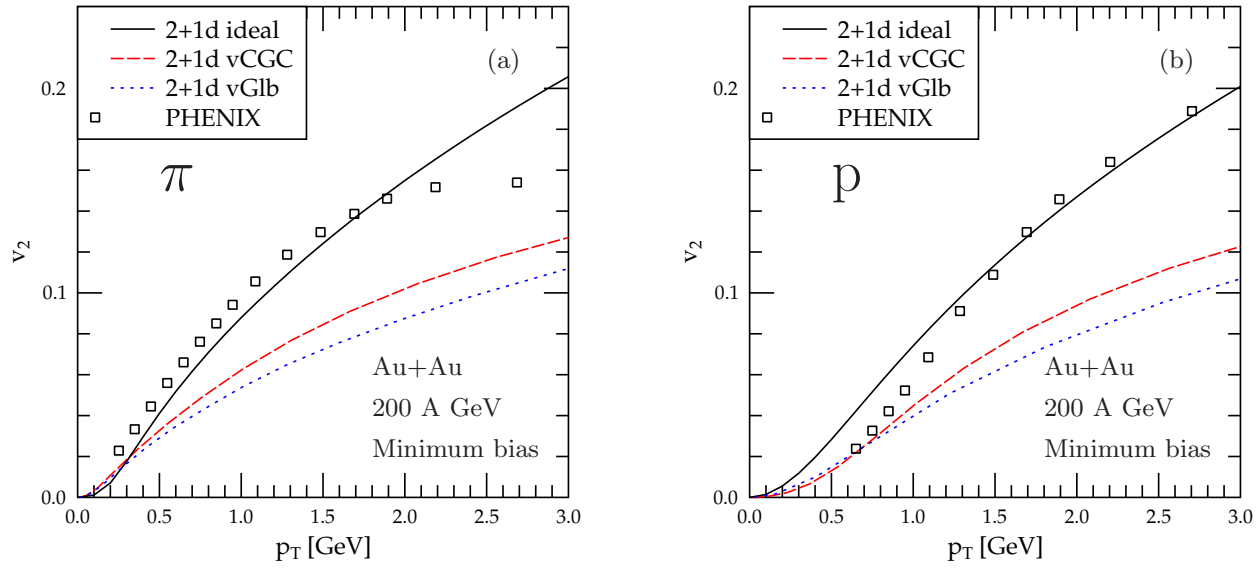

FIG. 2: (Color online) Elliptic flow of (a) charged pions and (b) protons in minimun bias 200 A GeV Au-Au collisions. Data from the PHENIX Collaboration [40] are shown without error bars since errors are smaller than the symbol size.

small contribution to this effect.

The p_T-dependent pion and proton elliptic flow from minimum bias Au-Au collisions at $\sqrt{s} = 200\,A$ GeV is shown in Fig. 2. Here the viscous calculations are seen to badly underpredict the measured values, as a consequence of shear viscous suppression of flow anisotropies [17, 35, 36]. The disagreement is not quite as bad for the CGC initial conditions which have somewhat larger initial spatial eccentricity $\varepsilon_x = \frac{\langle\langle y^2-x^2\rangle\rangle}{\langle\langle y^2+x^2\rangle\rangle}$ [37, 38] where

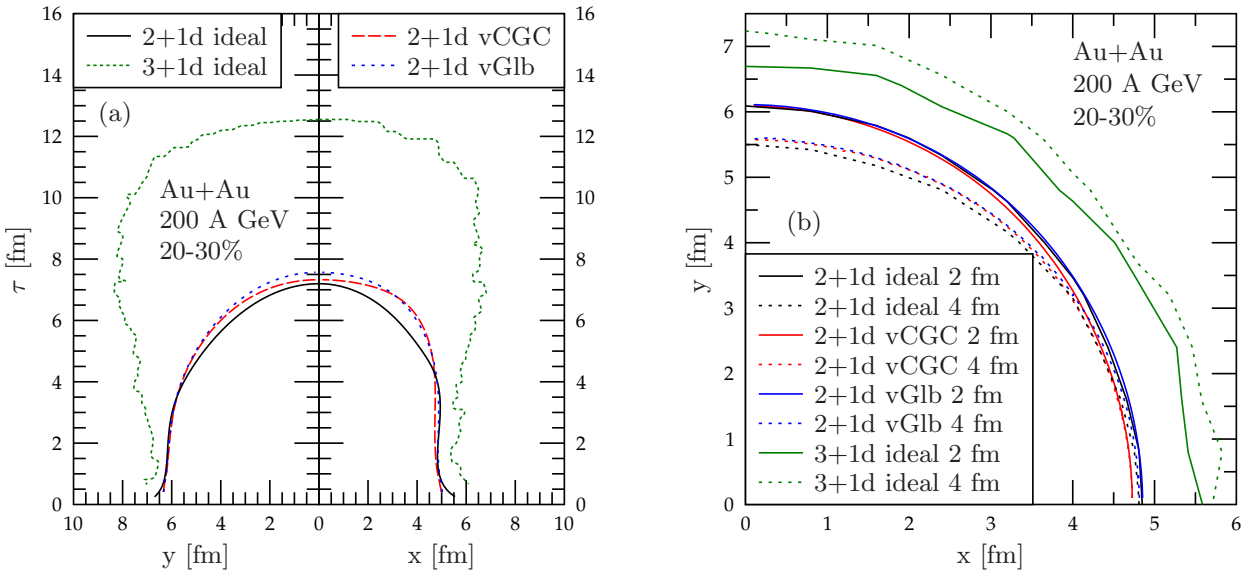

FIG. 3: (Color online) Freeze-out surfaces of the different hydrodynamic models in the (a) r-τ and (b) x-y planes for 200 A GeV Au-Au collisions in the 20-30% centrality class. The two halves of panel (a) show cuts through the freeze-out surface along the in-plane (x) and out-of-plane (y) directions, respectively. In panel (b), solid (dashed) lines represent cuts at $\tau = 2\,\mathrm{fm}/c$ ($4\,\mathrm{fm}/c$). The contours for the three (2+1)-d hydrodynamic models are almost indistinguishable.

$\langle\langle \dots \rangle\rangle$ denotes an average over the energy density in the transverse plane. But even in this case, the chosen value $\eta/s = 0.2$ yields too much suppression of v_2, in agreement with the findings in [37]. We found in [21] that for hydrodynamical models with smooth initial conditions quite generally the measured flatness of the proton p_T-spectra and the large elliptic flow $v_2(p_T)$ are in tension with each other, the former preferring larger η/s whereas the latter likes smaller viscosities.[3] We here chose to optimize the slope of the proton spectra, i.e. the magnitude of radial flow.

D. Geometry of the hydrodynamic fireballs

The different initial and final conditions, equations of state and viscosities assumed in the different hydrodynamical fireball models lead to some differences in the space-time evolution of the size and shape of the fireball which, weighted with the corresponding density distributions, affect the parton energy loss and its directional dependence. Figure 3 shows the freeze-out surfaces for Au-Au collisions in the 20-30% centrality class ($b = 7.49\,\mathrm{fm}$) in the r-τ and x-y planes. The different shapes of the freeze-out contours along the x and y directions in Fig. 3(a) reflect the elliptical source deformation in non-central collisions. Figure 3(b) shows freeze-out contours in the x-y plane at times $\tau = 2\,\mathrm{fm}/c$ (solid) and $\tau = 4\,\mathrm{fm}/c$ (dashed), illustrating how the out-of-plane elongation of the source decreases with time.[4]

The most striking feature of these contour plots is the similarity of the freeze-out contours for the three (2+1)-dimensional models. Even though the starting time τ_0 for the viscous simulations ($0.4\,\mathrm{fm}/c$) is more than twice as large as that used in the (2+1)-d ideal runs ($0.17\,\mathrm{fm}/c$), and the viscous fluid is allowed to cool down to $T_{\mathrm{dec}} = 130\,\mathrm{MeV}$ (compared to $T_{\mathrm{dec}} = 160\,\mathrm{MeV}$ for the (2+1)-d ideal runs), all three models complete their freeze-out almost at the same time ($\approx 7.2 - 7.5\,\mathrm{fm}/c$ for $b = 7.49\,\mathrm{fm}$). This is due to the additional radial flow produced by shear viscous pressure and the use in the viscous flow simulations of EoS s95p-PCE which is stiffer around the phase transition than the EoS used in the ideal fluid simulations [21]. The combination of these two effects allows the viscous fireball to cool faster during the late evolution stages and thus freeze out sooner than an ideal fluid with the same initial conditions [17].

During the early stages, on the other hand, viscous

[3] We do not know whether this statement remains true if fluctuating initial conditions are taken into account.

[4] The freeze-out surfaces extracted from the hydrodynamic output from the (3+1)-d simulations are wiggly due to numerical effects related to the fact that these simulations were done in Lagrangian coordinates.

heating delays the cooling process, so at early times (up to about 4 fm/c) the fireball center remains hotter and denser in the viscous case than for the ideal fluid.[5] The somewhat steeper initial density gradients of the CGC-fKLN profile (see Fig. 1 in [21]) generate slightly larger radial flow in the vCGC model, causing it to fully decouple a fraction of a fm/c earlier than the vGlb model.

Compared to the (2+1)-d simulations, the space-time volume covered by the ideal (3+1)-d fluid is much larger (wiggly green lines in Fig. 3). This not a consequence of dramatically different transverse expansion in (3+1)-d and boost-invariant (2+1)-d evolution (near midrapidity the longitudinal density profiles and expansion velocities in the (2+1)-d and (3+1)-d simulations are very similar), nor is it primarily due to starting the (3+1)-d simulation later (at $\tau_0 = 0.6\,\mathrm{fm}/c$). The main reason is that the (3+1)-d simulations use a bag model EoS with a first order phase transition that produces a relatively long-lived mixed phase where the speed of sound vanishes and the fluid stops accelerating.

III. PARTON-MEDIUM INTERACTION MODELS

In this work, we use two different models for the parton-medium interaction. The first is the Armesto-Salgado-Wiedemann (ASW) model of medium-induced radiative energy loss in perturbative Quantum Chromodynamics (pQCD), in the formulation of energy-loss probability distributions, so-called 'quenching weights' [41]. As characteristic for similar perturbative models of medium-induced radiation, it leads to a quadratic dependence of mean energy loss with the in-medium path length L in a constant medium due to the LPM suppression of subsequent radiation processes. We have picked this model among other formulations of radiative energy loss, since it shows the strongest path length dependence for $R_{AA}(\phi)$ of all radiative energy loss models tested in the same hydrodynamical background [6].

Note that the connection between LPM suppression and L^2 pathlength strictly appears in the limit of infinite parton energy in which the ASW model is derived. For the experimental kinematics, there is reason to expect that finite energy [42, 43] or finite size corrections [44] limit the L^2 domain to early times.

The second model is based on strong-coupling ideas for the medium. It is a hybrid model, in which the hard scales in the process are treated perturbatively, as in the standard pQCD radiative energy loss calculations, while the interaction with the plasma which involves strong-coupling dynamics is modeled based on AdS/CFT considerations for the $N=4$ super-Yang-Mills (SYM) theory [45]. In a constant medium, this phenomenological approach suggests an L^3 dependence of mean energy loss [46]. In the following, we will refer to this approach by the label 'AdS'.

We have refrained from testing a third class of models of energy loss by elastic scattering of a hard parton with medium constituents, which, as such scatterings are incoherent, would result in a linear dependence on the path length L in a constant medium. However, a large contribution of such processes to the total energy loss can be ruled out already by the data for $R_{AA}(\phi)$ [47, 48].

A key quantity in both models is the quenching weight, i.e. the energy loss probability distribution $P(\Delta E)$ given the path of a parton through the medium. In both models this is obtained by calculating the integrated virtuality transfer from the medium to the hard parton Q_s^2 and the characteristic medium-induced gluon energy ω_c by line integrals along the hard parton trajectory through the medium. Making use of a scaling law [49], we use Q_s and ω_c with the numerical results of [41] to obtain $P(\Delta E|\omega_c, Q_s) \equiv P(\Delta E)_{\mathrm{path}}$. What is different between the two models is the argument of the line integrals.

In the ASW model the medium is characterized by a transport coefficient $\hat{q}$ which measures the ability of the medium to transfer virtuality per unit path length. We assume that this can be written as a function of the medium thermodynamic parameters and parton position along the trajectory ξ via the relation

$$\hat{q}(\xi) = K \cdot 2 \cdot \epsilon^{3/4}(\xi)\big(\cosh\rho(\xi) - \sinh\rho(\xi)\cos\alpha(\xi)\big) \quad (3)$$

between the local transport coefficient $\hat{q}(\xi)$ (specifying the quenching power of the medium), the energy density ϵ and the local flow rapidity ρ with angle α between flow and parton trajectory [50, 51]. We view the parameter K as a tool to account for the uncertainty in the selection of the strong coupling α_s and possible non-perturbative effects increasing the quenching power of the medium (see discussion in [52]) and adjust it such that the pionic R_{AA} measured in central Au-Au collisions is reproduced.

With this expression for $\hat{q}$, we evaluate for each path through the medium (given by the initial vertex position $\boldsymbol{r}_0 = (x_0, y_0)$ in the transverse plane and the angle ϕ of the outgoing parton with the reaction plane) the line integrals

$$Q_s(\boldsymbol{r}_0, \phi) \;\equiv\; \langle \hat{q} L \rangle = \int d\xi\, \hat{q}(\xi), \quad (4)$$

$$\omega_c(\boldsymbol{r}_0, \phi) \;=\; \int d\xi\, \xi\, \hat{q}(\xi). \quad (5)$$

In the AdS model, these expressions are changed into [45]

$$Q_s(\boldsymbol{r}_0, \phi) \;=\; K \int d\xi\, \xi\, T^4(\xi), \quad (6)$$

$$\omega_c(\boldsymbol{r}_0, \phi) \;=\; K \int d\xi\, \xi^2\, T^4(\xi), \quad (7)$$

where $T(\xi)$ the local temperature of the medium and K is again a (different) free parameter, to be adjusted

[5] This information is not contained in Fig. 3 but can be verified by consulting Ref. [17].

such that the pionic R_{AA} for central Au-Au collisions is reproduced.

From the energy loss distribution for a given single path we can define the averaged energy loss probability distribution for a given angle ϕ as

$$\langle P(\Delta E)\rangle_\phi = \int_{-\infty}^{\infty} dx_0 \int_{-\infty}^{\infty} dy_0\, P(x_0,y_0)\, P(\Delta E)_{\rm path}, \quad (8)$$

where for given impact parameter $\boldsymbol{b}$ the probability density of hard vertices in the transverse plane $P(x_0,y_0)$ is given by the product of the nuclear profile functions as

$$P(x_0,y_0) = \frac{T_A(\boldsymbol{r}_0+\boldsymbol{b}/2)T_A(\boldsymbol{r}_0-\boldsymbol{b}/2)}{T_{AA}(\boldsymbol{b})}, \quad (9)$$

and the nuclear thickness function is given in terms of the Woods-Saxon nuclear density $\rho_A(\boldsymbol{r},z)$ as

$$T_A(\boldsymbol{r}) = \int dz\, \rho_A(\boldsymbol{r},z). \quad (10)$$

We calculate the momentum spectrum of hard partons in leading order perturbative QCD (LO pQCD) (explicit expressions are given in [52] and references therein). The medium-modified perturbative production of hadrons at angle ϕ can then be computed from the expression

$$\frac{d\sigma^{AA\to h+X}_{med}}{d\phi} = \sum_f \frac{d\sigma^{AA\to f+X}_{vac}}{d\phi} \otimes \langle P(\Delta E)\rangle_\phi \otimes D^{vac}_{f\to h}(z,\mu_F^2), \quad (11)$$

with $D^{vac}_{f\to h}(z,\mu_F^2)$ the fragmentation function with momentum fraction z at scale μ_F^2 [53]. From this we compute the nuclear modification function R_{AA} vs. reaction plane as

$$R_{AA}(P_T,y,\phi) = \frac{dN^h_{AA}/dP_T dy d\phi}{T_{AA}(\boldsymbol{b})\, d\sigma^{pp}/dP_T dy d\phi}. \quad (12)$$

The suppression of back-to-back high-p_T hadron correlations is computed in a Monte-Carlo (MC) framework [54]. We start from the expression for the production of two hard partons k,l in LO pQCD which is described by

$$\frac{d\sigma^{AB\to kl+X}}{dp_T^2 dy_1 dy_2} = \sum_{ij} x_1 f_{i/A}(x_1,Q^2) x_2 f_{j/B}(x_2,Q^2) \frac{d\hat{\sigma}^{ij\to kl}}{d\hat{t}} \quad (13)$$

where A and B stand for the colliding objects (protons or nuclei) and $y_{1(2)}$ is the rapidity of parton $k(l)$. The distribution function of a parton type i in A at a momentum fraction x_1 and a factorization scale $Q\sim p_T$ is $f_{i/A}(x_1,Q^2)$. The distribution functions are different for free protons [55, 56] and nucleons in nuclei [57, 58]. The fractional momenta of the colliding partons i, j are given by $x_{1,2} = \frac{p_T}{\sqrt{s}}(\exp[\pm y_1] + \exp[\pm y_2])$.

By sampling this expression, we generate events of back-to-back parton pairs which are placed on a vertex sampled according to Eq. (9) for given orientation ϕ with respect to the reaction plane. Given $(\boldsymbol{r}_0,\phi)$, we compute $P(\Delta E)$ for both partons according to the procedure outlined above and sample the distribution to obtain the energy loss for the given event.

Finally, we convert the simulated partons into hadrons. Note that this cannot be done using a fragmentation function as in Eq. (11) since $D^{vac}_{f\to h}(z,\mu_F^2)$ takes a hadronic energy scale μ_F as argument and measures the inclusive hadron yield, whereas we are interested in the yield of leading hadrons given a partonic energy scale.

More precisely, in order to determine if there is a trigger hadron above a given threshold, given a parton k with momentum p_T, we need to sample $A_1^{k\to h}(z_1,p_T)$, i.e. the probability distribution to find a hadron h from the parton k where h is the most energetic hadron of the shower and carries the momentum $P_T = z_1\cdot p_T$. In the following, we make the assumption that the hadronization process itself, at least for the leading hadrons of a shower, happens well outside the medium. As a consequence, we neglect any interaction of formed hadrons with the medium. The time scale for hadronization of a hadron h in its rest frame can be estimated by the inverse hadron mass, $\tau_h\sim 1/m_h$; boosting this expression to the lab frame one finds $\tau_h\sim E_h/m_h^2$. Inserting a hard scale of 6 GeV or more for the hadron energy and the pion mass in the denominator (as pions constitute the bulk of hadron production), this assumption seems well justified. We extract $A_1(z_1,p_T)$ and the conditional probability $A_2(z_1,z_2,p_T)$ to find the second most energetic hadron at momentum fraction z_2 *given that the most energetic hadron was found with fraction* z_1 from HERWIG [59]. After hadronization, we check if the most energetic hadron fulfills a given trigger condition and, if yes, we count the yield in various momentum bins of hadrons back-to-back with the trigger. Finally, we obtain the suppression factor $I_{AA}(\phi)$ for given trigger and associate momentum windows by dividing by the per-trigger yields found with nucleon parton distributions [55, 56] in the absence of a medium. The procedure is described in detail in [54].

IV. THE BULK FLUID MEDIUM EVOLUTION 'SEEN' THROUGH HARD PROBES

Hard partons undergoing energy loss do not probe the same properties of the bulk medium as soft hadrons, or they probe them in a different way. For example, while the coefficient v_2 in the soft sector measures pressure gradients translating an initial spatial anisotropy in non-central collisions into a momentum-space anisotropy, the same coefficient for high P_T hadrons measures directly the spatial anisotropy through the different energy loss induced by different densities seen by hard partons as a function of their angle with the reaction plane. This difference in the underlying physics is the reason why we prefer to present and discuss our results in terms of $R_{AA}(\phi)$ rather than in terms of the mean R_{AA} and v_2 at high P_T for a centrality class. While both choices contain

the same information, we feel that $R_{AA}(\phi)$ emphasizes the underlying suppression process.

To give a second example, while m_T-spectra of soft hadrons are rather sensitive to the late-time hadronic evolution of the medium and the amount of flow created during the hadronic evolution, the medium modification of hard probes is not at all sensitive to late time dynamics. The reason is that hard partons propagate through the medium with the speed of light, and thus typically escape from the medium at time scales of order of the size of the overlap region. This is especially true for observed hadrons, which have a bias to be produced relatively close to the surface [52].

In the following, we discuss some features of hydrodynamical models that are likely candidates to be probed by energy loss.

A. Medium properties potentially probed by energy loss

As apparent from Eqs. (4) to (7), the medium is probed by the energy loss models through path-length-weighted line integrals over the medium energy density ϵ or temperature T. The value of these integrals thus depends on

- the lower limit of the integral, corresponding to the time at which secondary particle production starts to be important enough to induce energy loss. Usually, the equilibration time τ_0 of the hydrodynamical model is used here, but there is no reason in principle why a non-equilibrated medium, if sufficiently dense, could not induce energy loss. However, the sensitivity to the lower limit is expected to be comparatively weak, as factors of ξ or ξ^2 in the ω_c integrals suppress this region. In a Bjorken model, $\hat{q}$ would diverge as $1/\xi$ for small times, thus cancelling a factor ξ of the suppression. However, prior to equilibration the density of particles in the medium off which the hard parton can scatter, thereby inducing it to radiate gluons, must generically be smaller than in thermal equilibrium (which maximizes entropy and is thus a state of maximum particle density for given energy density), so this cancellation cannot be perfect, and we expect (within reasonable limits) a weak sensitivity to the choice of the initial time.

- the upper limit of the integral, corresponding to the time scale at which the hard parton is no longer surrounded by a medium. This is usually assumed to be given by the location of the Cooper-Frye surface in a hydrodynamical model beyond which the medium is no longer coupled but free-streaming. The Cooper-Frye surface in turn is often defined to be an isothermal surface. Since the Cooper-Frye prescription is clearly an idealization of the real physics of the system boundary, there is again no strong reason to identify the upper integration boundary with this surface, as there could be energy loss of a parton in a weakly coupled hadronic halo. However, again in practice the sensitivity to the detailed choice of the parameter is parametrically weak. While the factors ξ or ξ^2 tend to enhance late-time contributions to the integral, the medium density at late times or large distances from the center dilutes eventually like $1/\xi^3$, due to both longitudinal and transverse flow. Thus, beyond a point we do not expect that our results depend strongly on the medium boundary choice.

- the functional form of the integrand itself. Note that what is probed by the parton is not the medium density at any given proper time, but rather the medium density along the light cone. However, since interference effects suppress early time energy loss and the onset of transverse flow suppresses late time energy loss, effectively the mean energy loss per unit time dE/dx reaches a relatively sharp maximum around $\tau_{\rm peak} \sim 3-4$ fm/c (cf. [60]). Thus, to first approximation, energy loss probes the density distribution of the medium around $\tau_{\rm peak}$. In particular, this implies that there is a finite time for processes like viscous entropy production or decay of the spatial deformation by pressure-generated anisotropic flow to modify the state of the system before it is probed by energy loss.

- finally, when comparing the distribution (9) of primary production vertices with any transverse distribution of matter in a hydrodynamical model, one will find that there is always a non-zero probability to find a hard vertex outside the medium and hence partons which never experience energy loss. Since such 'halo-partons' never probe the medium, they show no correlation with the reaction plane angle ϕ and hence their presence will dilute any dependence of R_{AA} on ϕ. This effect scales with the size of the hydrodynamical medium, i.e. with the assumed initial extent of the Cooper-Frye surface. For very large media this 'halo effect' is suppressed, but for drastic assumptions (such as energy loss only in the QGP) it is not negligible.

In the following, we will discuss these points in more detail in the context of different hydrodynamical models.

B. Viscous entropy production

In both ideal and viscous fluid dynamics, the entropy of the final state is fixed by the observed multiplicity and chemical composition of the emitted hadrons. But only in ideal fluid dynamics this final entropy agrees with its initial value. In viscous hydrodynamics, viscous heating causes the entropy to increase with time, which implies that, for the same final multiplicity, the viscous fluid

starts at lower entropy and parton density than the ideal fluid. The rate of viscous entropy production grows with the expansion rate of the fireball. A boost-invariant longitudinal expansion profile, as initially assumed in all versions of the hydrodyamic model studied here, leads to an expansion rate that diverges like $1/\tau$ at early times τ. Thus, most of the viscous entropy production happens near the beginning of the expansion [17]. Viscous heating causes the fireball density to decrease initially more slowly with time than for an ideal fluid. This has implications for the density profile seen by a hard parton propagating on the lightcone.

We illustrate this effect in Fig. 4 where we show the integrand of Eq. (5), $\xi\,\hat{q}(\xi)$, as a function of ξ for a parton propagating in-plane from the medium center in a hydrodynamical background corresponding to Au-Au collisions at impact parameter $b = 7.49\,\mathrm{fm}$, for four different hydrodynamical models.

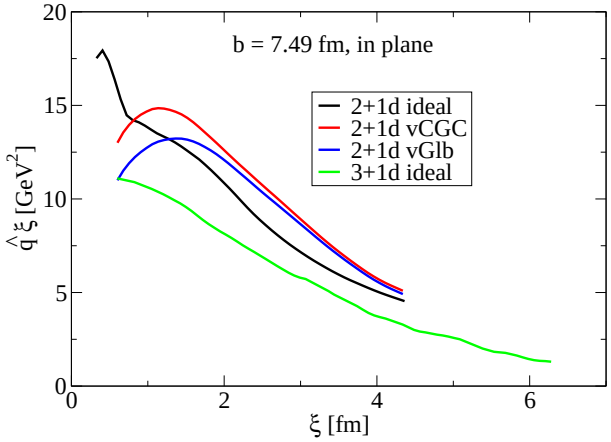

FIG. 4: (Color online) The integrand of Eq.(5) as a function of parton distance ξ along the light-cone for four different hydrodynamical models, shown for a parton propagating in-plane from the fireball center.

While the ideal hydrodynamical models show a monotonical decrease for $\xi\,\hat{q}(\xi)$, the viscous models show an initial rise due to viscous entropy production, followed by a decrease due to flow-driven density dilution. This means that in viscous hydrodynamical models energy loss is generically somewhat shifted to later times.

Note also that due to the lower entropy in the initial state in viscous hydrodynamics, if one wants to get the same R_{AA}, the factor K in Eqs. (3), (6), (7) must be larger (by about a factor 2 for the models presented here) than in an ideal fluid model that leads to a similar final state.

C. Line integral limits

As discussed above, there is no compelling reason why the hydrodynamical thermalization time should be equal to the initial time of energy loss, nor why the Cooper-Frye decoupling surface for soft hadrons should coincide with the boundary beyond which the hard parton no longer interacts with the medium.

In order to test the sensitivity of our results to choices of these parameters different from the hydrodynamical values, without explicitly modeling the (rather complicated) dynamics prior to thermalization or the perturbative scattering of hard quarks or gluons with hadrons in the halo, we adopt the following procedure: We probe the response of the system to variations of the hydrodynamical starting time τ_0 and of the final temperature T_F, with the understanding that these parameters are not meant as physically reasonable choices within the hydrodynamical framework, but rather serve to generate upper limits for the true conditions — certainly prior to thermalization the actual energy density will be less than in the hydrodynamical extrapolation to early times. In that sense, the parameters τ_0 and T_F are to be understood in this subsection as the initial energy loss time and the equivalent temperature corresponding to the edge of the medium that contributes to energy loss.

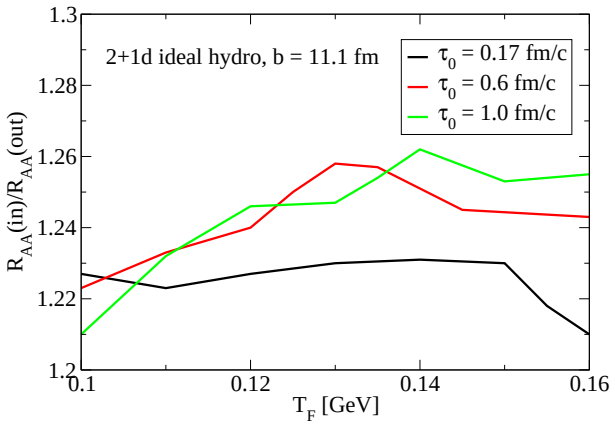

FIG. 5: (Color online) The ratio of $R_{AA}(\phi=0)/R_{AA}\left(\phi=\frac{\pi}{2}\right)$ for various combinations of the initial energy loss time τ_0 and the equivalent temperature T_F of the medium edge, for the case of the (2+1)-d ideal fluid model.

In Fig. 5 we show the results of a variation of τ_0 and T_F on the observable spread between the in-plane and out-of-plane emission, for the case of the (2+1)-d ideal hydrodynamical model. While the variation looks optically significant, it is small on an absolute scale (note the suppressed zero!), at most 15% from the mean. This is less than, for example, the variation between different hydrodynamical models. This in itself is certainly reassuring, as it quantifies the uncertainty in choosing the proper line integral limits. It is also readily apparent that the spread is typically maximized for 'reasonable' choices of the freeze-out temperature, thus there is no evidence for a need to choose dramatically different last-scattering surfaces for soft and hard particles.

Note that there is a systematic trend that large τ_0 (i.e. delayed parton energy loss) leads to an increased in-plane vs. out-of-plane spread. This fits well into a pattern that

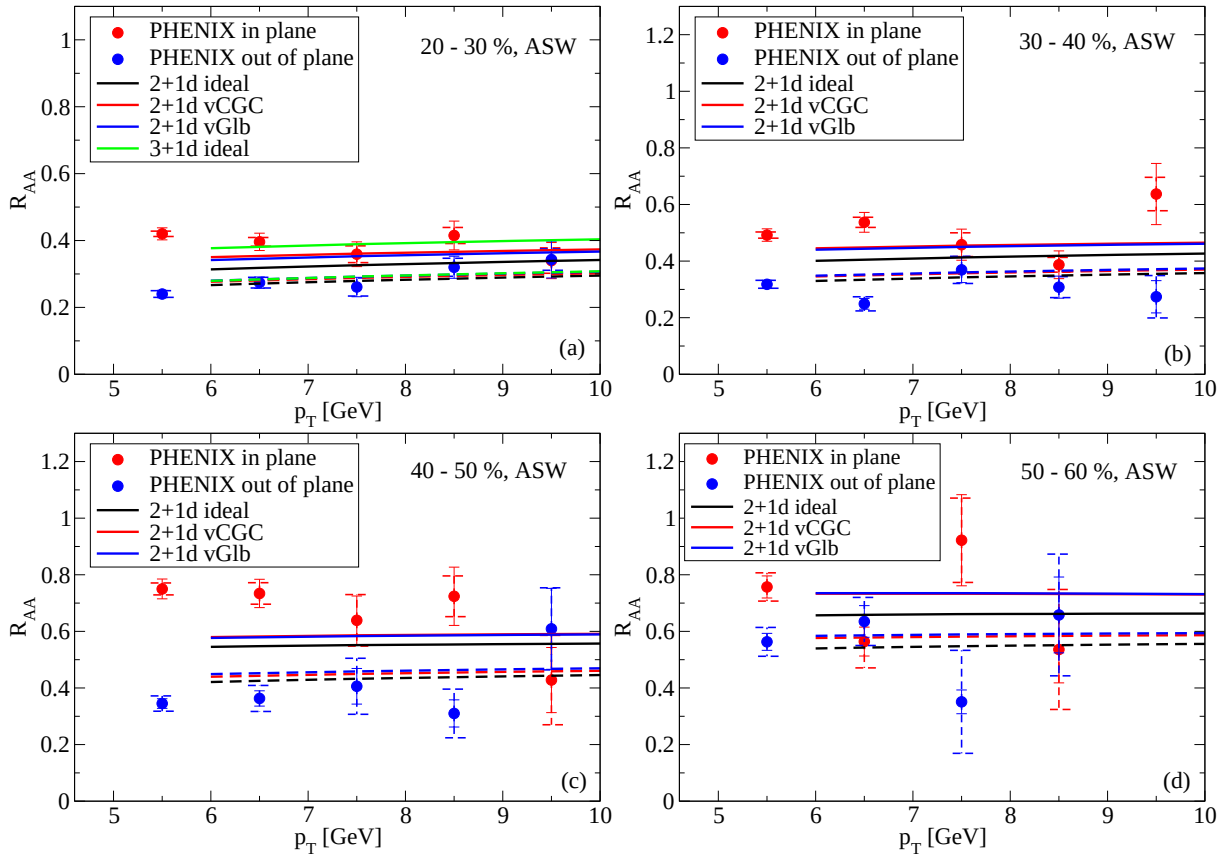

FIG. 6: (Color online) The nuclear suppression factor R_{AA} as a function of P_T, shown in plane (solid) and out-of-plane (dashed). The calculation was done with the ASW perturbative radiative energy loss model for different hydrodynamical descriptions for the medium, describing 200 A GeV Au-Au collisions in four different centrality classes. PHENIX data [61] are shown for comparison.

shifting the strength of the mean energy loss per unit length dE/dx to later times leads to an increased ratio of out-of-plane vs. in-plane suppression. We will return to this issue in more detail later.

V. RESULTS

In order to illustrate how the differences between the media computed with different hydrodynamical models are probed by energy loss, we show results for R_{AA} for in-plane and out-of-plane emission for various collisions centralities, using both the ASW and AdS energy loss frameworks and comparing with PHENIX data [61]. In all calculations, a single free parameter K has been adjusted such that a good description of R_{AA} in 0-10% most central collisions is achieved. We therefore refrain from showing any results for central collisions, as they are virtually identical for all models.[6]

In Fig. 6 we show results for the ASW energy loss models from mid-peripheral collisions in the 20-30%, 30-40%, 40-50% and 50-60% centrality classes. While all hydrodynamical models reproduce well the centrality dependence of the angular averaged (mean) R_{AA} value, showing very weak P_T-dependence, the spread between in-plane and out-of-plane emission appears generally too small (with the possible exception of the (3+1)-d ideal fluid model). This is especially apparent in the 40-50% centrality class. Note that the successful description of the centrality dependence of the mean R_{AA} is not trivial, since this probes the path length dependence of energy loss: in an elastic energy loss model with linear L dependence, even the mean R_{AA} does not correctly extrapolate from central to peripheral collisions [48].

Fig. 7 shows a similar comparison as Fig. 6 for the strong coupling AdS energy loss model which features a stronger L dependence than the ASW model ($\sim L^3$ instead of $\sim L^2$). Here there is a tendency for the mean R_{AA} to lie above the more peripheral data, but the spread

[6] This is related to the point made already in [10] that R_{AA} is practically insensitive to the functional form of the energy loss probability distribution $P(\Delta E)$ beyond its first moment.

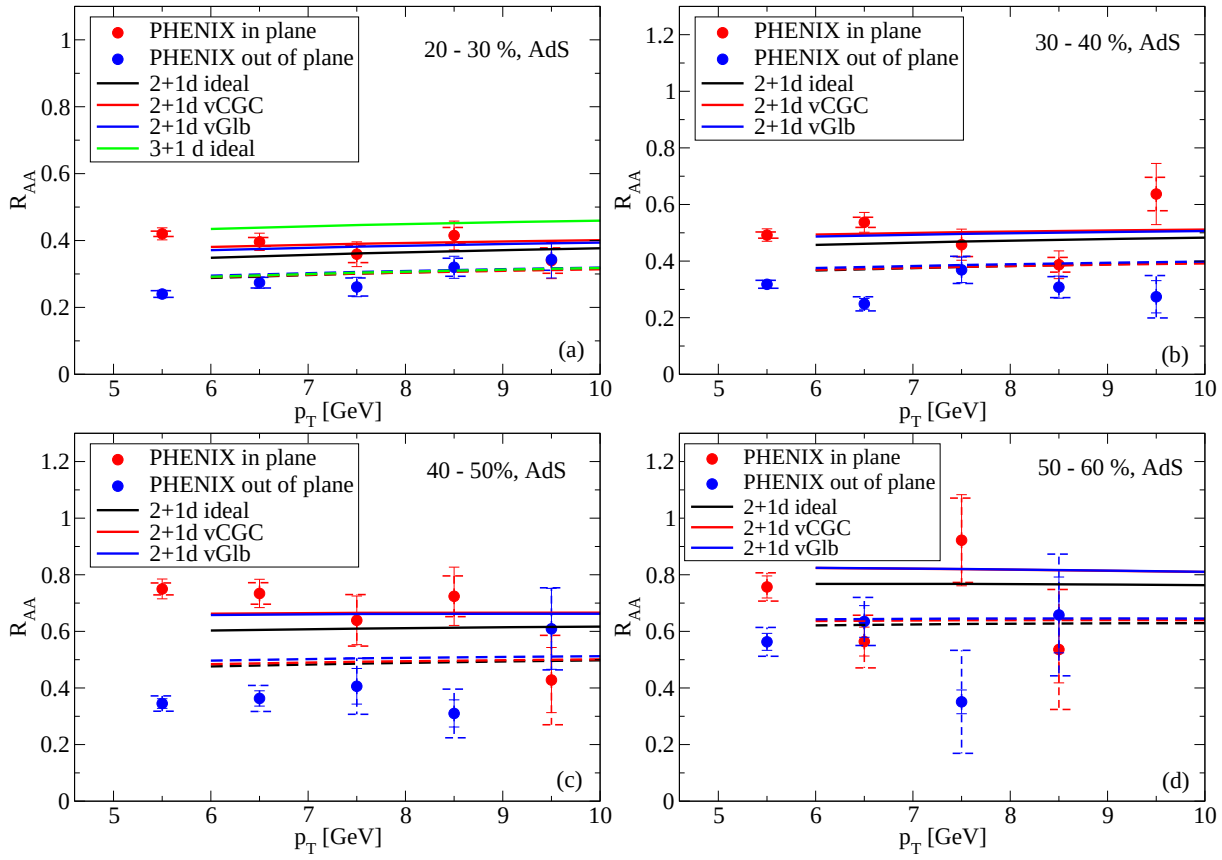

FIG. 7: (Color online) Same as Fig. 6 except that the calculation was done with the AdS strong coupling radiative energy loss model.

between in-plane and out-of-plane emission is generically larger and agrees better with the data.

Let us comment on some trends: In all cases, the in-plane emission shows a stronger dependence on the underlying hydrodynamical model than the out-of-plane emission. This is to be expected, as the conditions for emission out-of-plane (e.g. in terms of average in-medium path length) are always more similar to the conditions in central collisions where in all models K has been adjusted to describe the data, whereas the conditions for emission in the reaction plane change more strongly with centrality.

The relatively small difference between fireballs resulting from CGC and Glauber initial states is rather remarkable. Given the stronger spatial anisotropy of the CGC initial state, one would expect to see this reflected in the anisotropy in high P_T parton energy loss. The solution to this puzzle seems to lie in the observation made earlier that energy loss probes the system at a timescale of $\sim 3-4$ fm, i.e. after the stronger pressure gradients of the CGC initial state already had some time to reduce the fireball eccentricity.

With regard to the magnitude of the spread between in-plane and out-of-plane emission, we observe that consistently the (3+1)-d ideal hydro leads to the largest spread, followed by the viscous hydro models with CGC and Glauber initial conditions, while the (2+1)-d ideal fluid medium results in the smallest spread. We stress at this point that this observation cannot be directly linked to explicit modeling of the dynamics in z-direction or to viscosity. We will discuss the causes for this ordering in the next section.

In Fig. 8 we show the suppression factor I_{AA} for the away-side yield in triggered back-to-back correlations with a trigger momentum range of $4-7$ GeV, using the ASW model. Note that the trigger range is *not yet* in a region where hadron production is dominated by the fragmentation of hard partons. It has been chosen to match with the range of an ongoing experimental analysis, keeping the mentioned caveat in mind.

For 20-30% centrality, our statistics is not good enough to even cleanly separate in-plane from out-of-plane emission. In the 50-60% centrality class, however, we essentially recover the ordering between models in the in-plane vs. out-of-plane spread observed before.

Going to the AdS model in Fig. 9, the overall magnitude of I_{AA} is somewhat different, but qualitatively the picture of the relative ordering of the spread between the different models remains unchanged. Given that computations of $I_{AA}(\phi)$ are rather involved and suffer from limited statistics, it is not clear that I_{AA} offers any real tomographic benefit over R_{AA}.

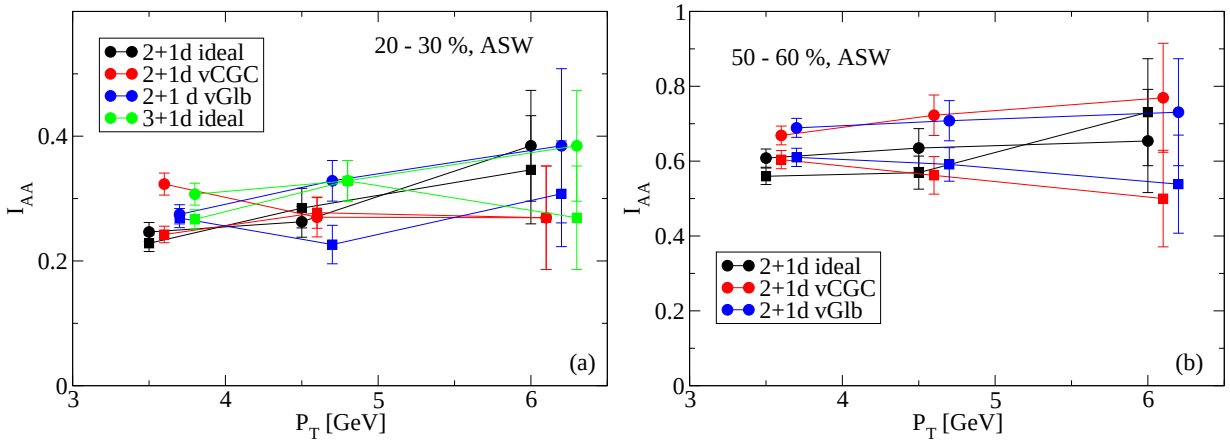

FIG. 8: (Color online) The suppression factor I_{AA} of the away-side per-trigger yield, calculated in the ASW perturbative radiative energy loss model for 4-7 GeV trigger momentum and shown as a function of the away-side momentum P_T. Squares show $I_{AA}(\phi=0)$ (in-plane), circles show $I_{AA}\left(\phi=\frac{\pi}{2}\right)$ (out-of-plane). Calculations are done for four hydrodynamical models for 200 A GeV Au-Au collisions for two different centralities.

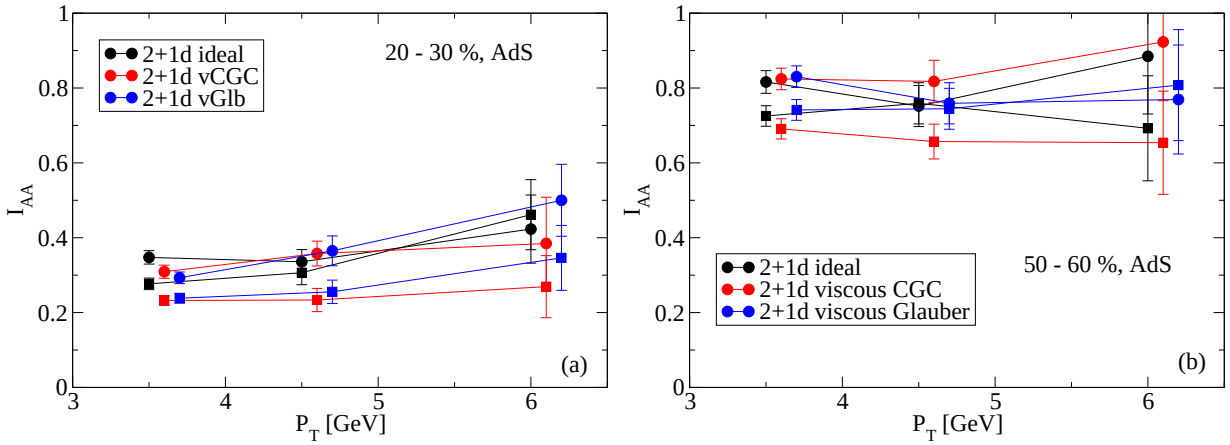

FIG. 9: (Color online) Same as Fig. 8 but for the AdS strong coupling radiative energy loss model.

In order to illustrate more clearly how the energy loss probes the medium density evolution, we show in Figs. 10 and 11 the conditional probability density to have the production vertex of the hard parton at position (x, y), given that a hard hadron was observed. We show calculations for the 20-30% centrality class using the ASW energy loss model; the qualitative features and differences between different hydrodynamical models seen in these plots repeat themselves in other centrality classes and are slightly enhanced for the AdS energy loss model which we do not show here.

In the absence of a medium, this production vertex density distribution is given by the binary collision distribution Eq. (9). The medium biases the distribution in a characteristic way towards the surface, as partons produced in the dense medium core are unlikely to escape with a significant fraction of their momentum left. The plots have been obtained by binning the distribution of triggered events in the MC code for the computation of back-to-back hadron correlations, but the same conditional $P(x, y)$ for the trigger distribution is also underlying the single hadron suppression R_{AA}.

As expected, the degree of surface bias is much larger for out-of-plane than for in-plane emission, reflecting the larger degree of suppression seen out-of-plane. Comparing the y-position of the maximal out-of-plane emissivity, a stronger degree of surface bias in the (2+1)-d ideal vs. the (3+1)-d ideal hydrodynamics is readily apparent. The two viscous models reflect their different density evolutions in a less straightforward way, for example in the different shape of the emissivity maximum or in the distortion of the outer contour lines. As previously observed in [52], there is no evidence for strictly surface-biased emission or a corresponding tangential bias. In all models, a significant fraction of observed hadrons originates from the medium core.

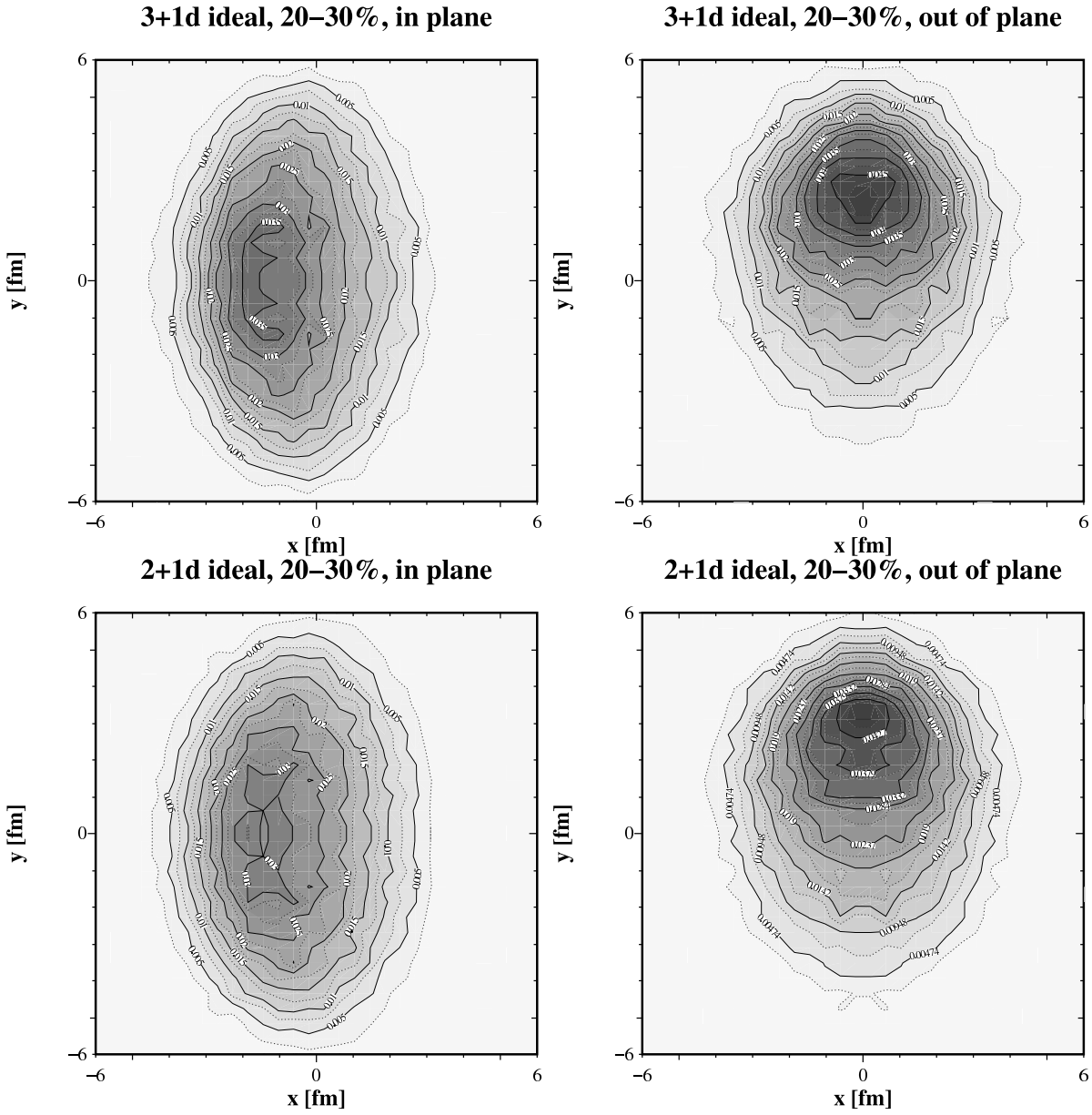

FIG. 10: Probability density of finding a parton production vertex at (x, y) in the transverse plane, given an observed hard hadron with $4\,\mathrm{GeV} < P_T < 7\,\mathrm{GeV}$. Calculations using the ASW energy loss model are shown for the (3+1)-d (top row) and (2+1)-d ideal hydrodynamical models (see text). In the case of in-plane emission (left panels) the hadron propagates to the $-x$ direction and we use $y \leftrightarrow -y$ symmetrization for the plot. In the case of out-of-plane emission the hadron propagates to the $+y$ direction and we used $x \leftrightarrow -x$ symmetrization. Countours are at linear intervals.

VI. INTERPRETATION OF THE RESULTS

Arguably the most important question in light of the magnitude of the measured spread between in-plane and out-of-plane emission is whether the data require a strong coupling description of energy loss along the lines of the AdS model or if, given a suitable description of the medium, perturbative QCD is able to account for the data. A related issue of similar importance is what constraints for hydrodynamical models can be derived from measurements of hard probes that cannot also be gained from bulk matter data.

Let us discuss these questions in view of our findings. It is a fortunate accident that the Cooper-Frye surfaces (see Fig. 3) of all (2+1)-d models studied here are almost identical. Since we can easily test how $R_{AA}(\phi)$ is changed when we make τ_0 (here denoting the starting time for energy loss) equal in these runs (cf. Fig. 5), we have practically eliminated any effect of different in-medium path lengths and can ascribe any differences in the resulting suppression patterns to the density distributions probed along the hard parton path.

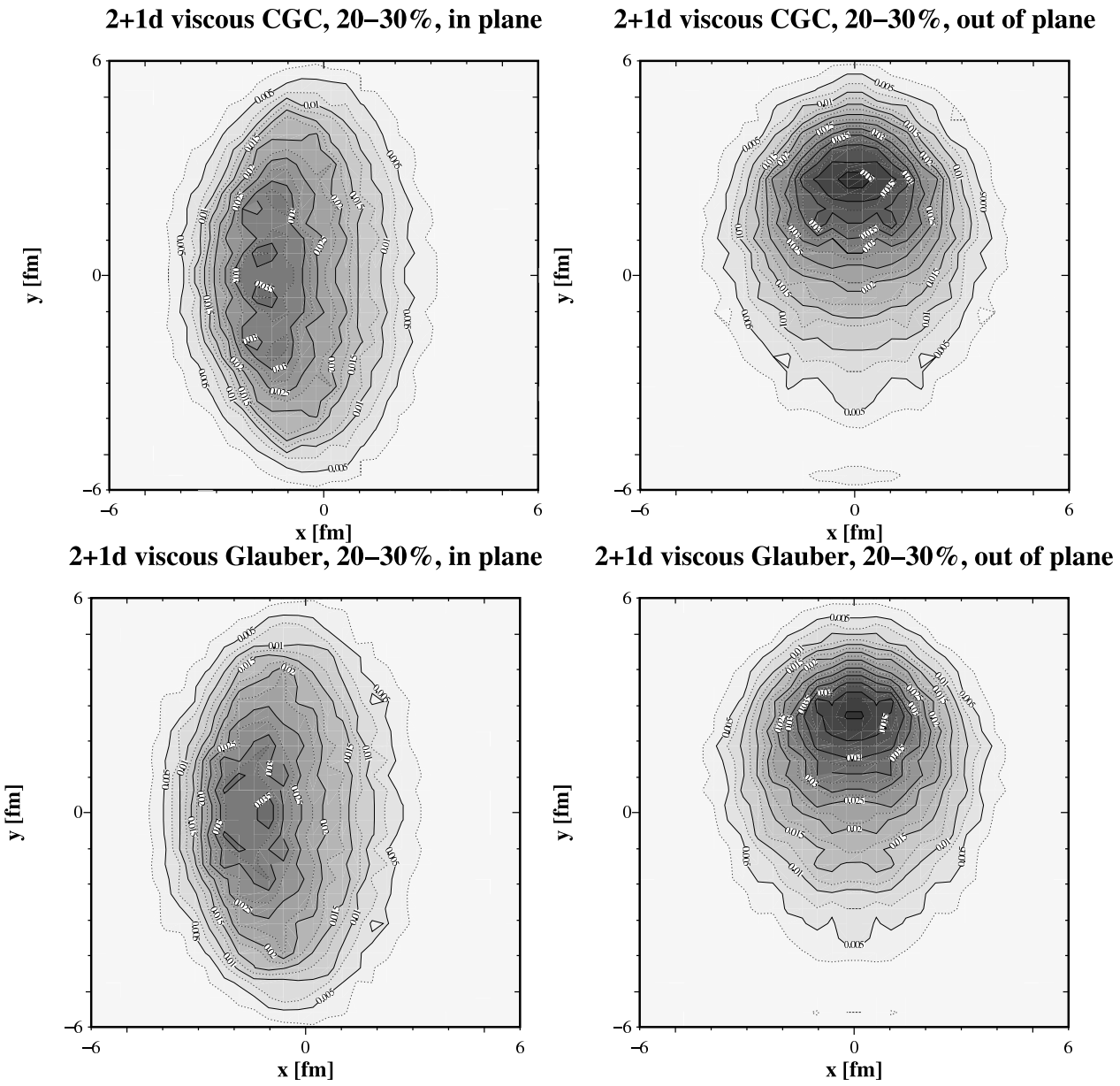

FIG. 11: Same as Fig. 10 but for the viscous hydrodynamical models with CGC-fKLN (top row) and Glauber (bottom row) initial conditions (see text).

We note that the (2+1)-d ideal and vGlb hydrodynamics both share (to good approximation) the same shape of the initial state whereas the vCGC hydrodynamics has a different initial state. This enables us to disentangle different contributions to the in-plane vs. out-of-plane spread: about 50% of the difference in spread between the (2+1)-d ideal and vCGC hydrodynamics shown in Fig. 6 can be ascribed to the difference in the initial time τ_0 (Fig. 5 indicates that a small τ_0 is strongly disfavoured), about 35% of the difference results from viscosity, and the remaining 15% are caused by the difference between CGC and Glauber initial profiles.

Turning to the (much larger) spread observed in the (3+1)-d hydrodynamics, we can surmise that most of the increase must arise from the different size of the freeze-out hypersurface as caused by the bag model EOS (and the resulting different distribution of in-medium path lengths and densities, which in this case is different from a re-adjustment of T_F). This in turn implies that, once the parameter K has been adjusted to yield the same mean R_{AA} as in the other models, the numerical value of $\hat{q}$ at each space-time point is much smaller in the (3+1)-d ideal hydro model than in the other models (see Fig. 4). Another way to state this is that in the (3+1)-d model partons travel on average a larger distance before they acquire the same amount of virtuality transfer from the medium.

The common theme in all these findings is that the

spread between in-plane and out-of-plane emission is increased whenever energy loss is shifted to later times. This may occur due to viscous heating during expansion, or in response to the choice of a large τ_0, or as the result of an L^3 path length weighting as in the AdS model — while the details differ, the net result is qualitatively the same in each of these cases. We note that this agrees qualitatively with the conclusions in [62] whose authors achieve a large in-plane vs. out-of-plane spread by requiring the hard parton to suffer the largest energy loss rate in a relatively thin shell of matter whose temperature is close to T_c.

This observed connection between the time dependence of energy loss and the in-plane vs. out-of-plane spread requires an explanation, especially in light of the fact that elliptic flow *decreases* the initial spatial anisotropy of the system over time. The key to understanding this phenomenon lies in the realization that the spatial anisotropy exists on a scale of the order of the spatial size of the transverse overlap region, i.e. several fm. It is thus a global property of the medium. If energy loss were significant only at very early times $\tau \lesssim 1\,\mathrm{fm}/c$ (as approximately true for elastic energy loss), it could not resolve any phenomenon on a distance scale $d \gg 1$ fm and would thus probe the medium properties only locally. In other words, in such a model most high p_T partons would be blind to the spatial anisotropy (see discussion in [47]), and consequently the observed spread would be very small.

While the above argument is strictly true only for a homogeneous medium, it still holds qualitatively for an inhomogeneous and hydrodynamically evolving medium: The spread between in-plane and out-of-plane emission increases not because energy loss is shifted to late times, but because the typical time scale over which energy loss is strong approaches the global spatial scales of the medium, and hence the partons are increasingly able to probe the medium globally.

Unfortunately this finding does not translate into straightforward constraints for the medium evolution model. Rather than being dominated by a single large effect, $R_{AA}(\phi)$ appears to be sensitive to a number of effects of roughly equal importance. However, while some constraints are qualitatively similar to what was found in the soft sector (for example, a CGC initial profile causes both a larger v_2 in the soft sector and a larger azimuthal variation of R_{AA} in the hard sector), others are qualitatively different and potentially more valuable (viscosity causes smaller v_2 for the bulk matter but a larger azimuthal variation of $R_{AA}(\phi)$).

Given that our results do not exhaust the parameter space of hydrodynamical evolutions compatible with bulk data, it is entirely conceivable that an evolution can be found for which both magnitude and spread of $R_{AA}(\phi)$ are described within pQCD dynamics. Presumably, a viscous (3+1)-d hydrodynamics with a CGC initial state, late thermalization and low freeze-out temperature would be a good candidate. At this point, we see no reason to conclude that the data require a strong-coupling model.

VII. SUMMARY

The goal of this paper was to develop a better understanding of the tomographic power of parton energy loss measurements in relativistic heavy-ion collisions as probes of the medium created in these collisions and/or of the mechanism by which hard partons lose energy in such a medium. To this end we presented a study of the dependence on the angle with the reaction plane ϕ of the nuclear suppression ratio $R_{AA}(\phi)$ and the away-side per-trigger yield $I_{AA}(\phi)$ in triggered back-to-back correlations, for four different hydrodynamic models of the fireball evolution and two different models for the path length dependence of parton energy loss. The models were tightly constrained by ensuring that parameters were chosen such that the soft-hadron transverse momentum spectra are well described for all collision centralities, and that all models yield the same nuclear suppression factor R_{AA} for pions in central Au-Au collisions. We then studied differences in the dependence of R_{AA} and I_{AA} on collision centrality, transverse momentum P_T, and azimuthal emission angle ϕ relative to the reaction plane.

We found that, after tuning the models to reproduce the correct pion R_{AA} in central collisions, they all gave approximately identical results for the collision centrality dependence of the azimuthally averaged $R_{AA}(P_T)$, featuring weak P_T-dependence and yielding good qualitative agreement with experimental data. The tomographic power of this azimuthally averaged quantity for distinguishing between different (realistic) medium models is therefore low. A stronger path length dependence of the energy loss ($\sim L^3$ instead of $\sim L^2$) produces a slightly stronger impact parameter dependence of the ϕ-averaged R_{AA}, but small differences between the different hydodynamic models for the medium interfere with this tendency, making it difficult to disentangle these effects. The centrality dependence of the azimuthally averaged I_{AA} is *a priori* a bit more promising since it was found to react more strongly to changes in the path length dependence of the energy loss. On the other hand, to measure this quantity with good statistical precision is much more difficult. Furthermore, it is not obvious from our studies that such a measurement will contribute any useful information about the medium that would help distinguish between different hydrodynamic evolution models. The azimuthally averaged R_{AA} is found to provide practically no such discriminating power.

The measurement of the in-plane vs. out-of-plane variation of $R_{AA}(\phi)$ provides much better discrimination.[7]

[7] Whether the same holds true for the azimuthal variation of I_{AA} depends on how large an oscillation amplitude will be found in

We confirm earlier findings that it is not easy to reproduce the relatively large oscillation amplitude of $R_{AA}(\phi)$ found by the PHENIX experiment. We identified several mechanisms that help to increase the in-plane vs. out-of-plane spread of R_{AA} and, in combination, may be able to explain the data: (i) A stronger path length dependence of parton energy loss, combined with (ii) a delayed beginning of the energy loss action, caused by the need for allowing the scattering centers in the medium that induce the hard parton to radiate energy to decohere from the initial state wave function of the colliding nuclei, (iii) a delay of the flow-induced dilution of the medium density by viscous heating, and (iv) a larger fireball eccentricity by intializing the hydrodynamic evolution with CGC-fKLN initial conditions rather than the less deformed Glauber model initial density profile. We found that the combination of effects (i) and (ii) accounts for about 50% of the azimuthal spread found in our calculations, viscous heating contributes another 35% of the effect, with the remaining 15% arising from different initial fireball eccentricities.

Analyzing the reasons why the mechanisms (i)-(iii) cause a larger in-plane vs. out-of-plane spread of R_{AA}, we found that they all shift the weight of the energy loss towards later times along the path of the parton. This allows the parton energy loss to probe the spatial anisotropy of the medium (which is a global fireball property) on a global length scale, rather than probing the properties of the medium locally in the vicinity of the production vertex only. If the global spatial anisotropy of the medium can be probed by a parton, the connection between spatial medium anisotropy and final state hard parton momentum anisotropy is strongest.

We would like to point specifically to the role of viscosity in this context: We are beginning to see significant roles played by the (necessarily non-zero) shear viscosity of the quark-gluon plasma even though its absolute value (expressed through the dimensionless ratio $\frac{\eta}{s} = \mathcal{O}(1-3) \times \frac{1}{4\pi}$) is almost as small as theoretically possible [63]. In [21] we found that $\frac{\eta}{s} \approx (2-3) \times \frac{1}{4\pi}$ gives the best fit to the pion and proton momentum spectra in 200 A GeV Au-Au collisions, and here we found that a similar value contributes significantly to the in-plane vs. out-of-plane spread of R_{AA} for pions. We hope and expect that a combined analysis of all RHIC data on soft hadron production *and* hard parton medium modification will eventually lead to an accurate determination of the quark-gluon plasma viscosity.

Acknowledgments

Discussions with Kari Eskola are gratefully acknowledged. This work was supported by an Academy Research Fellowship of T.R. from the Finnish Academy (Project 130472) and from Academy Project 133005. H.H. gratefully acknowledges the financial support from the national Graduate School of Particle and Nuclear Physics. The research of U.H. and C.S. was supported by the U.S. Department of Energy under contract DE-SC0004286 and within the framework of the JET Collaboration under grant number DE-SC0004104.

[1] M. Gyulassy, P. Levai and I. Vitev, Phys. Lett. **B538** (2002) 282.
[2] E. Wang and X. N. Wang, Phys. Rev. Lett. **89** (2002) 162301.
[3] C. A. Salgado and U. A. Wiedemann, Phys. Rev. Lett. **89** (2002) 092303.
[4] G. G. Barnafoldi, P. Levai, G. Papp, G. I. Fai and M. Gyulassy, Eur. Phys. J. C **33** (2004) S609.
[5] S. Wicks, W. Horowitz, M. Djordjevic and M. Gyulassy, Nucl. Phys. **A784** (2007) 426.
[6] S. A. Bass, C. Gale, A. Majumder, C. Nonaka, G. Y. Qin, T. Renk and J. Ruppert, Phys. Rev. C **79** (2009) 024901
[7] G. Y. Qin, J. Ruppert, C. Gale, S. Jeon, G. D. Moore and M. G. Mustafa, Phys. Rev. Lett. **100** (2008) 072301
[8] T. Renk and K. Eskola, Phys. Rev. C **75** (2007) 054910.
[9] B. Schenke, C. Gale and S. Jeon, arXiv:0911.4470 [hep-ph].
[10] T. Renk, Phys. Rev. C **74** (2006) 034906.
[11] A. Majumder, Phys. Rev. C **75** (2007) 021901.
[12] C. Nonaka and S. A. Bass, Phys. Rev. C **75** (2007) 014902.
[13] H. Holopainen, S. S. Räsänen and K. J. Eskola, to be published.
[14] P. F. Kolb, U. Heinz, P. Huovinen, K. J. Eskola, and K. Tuominen, Nucl. Phys. **A696** (2001) 197.
[15] M. Laine and Y. Schroder, Phys. Rev. D **73** (2006) 085009.
[16] F. Cooper and G. Frye, Phys. Rev. D **10** (1974) 186.
[17] H. Song and U. Heinz, Phys. Lett. B **658** (2008) 279; Phys. Rev. C **77** (2008) 064901; and Phys. Rev. C **78** (2008) 024902.
[18] H. Song and U. Heinz, Phys. Rev. C **81** (2010) 024905.
[19] W. Israel and J. M. Stewart, Annals Phys. **118** (1979) 341.
[20] A. Muronga, Phys. Rev. Lett. **88** (2002) 062302 [Erratum-ibid. **89** (2002) 159901]; and Phys. Rev. C **69** (2004) 034903.
[21] C. Shen, U. Heinz, P. Huovinen and H. Song, "Systematic parameter study of hadron spectra and elliptic flow from viscous hydrodynamic simulations of Au+Au collisions at $\sqrt{s_{\rm NN}} = 200\,{\rm GeV}$", to be published.
[22] P. Huovinen and P. Petreczky, Nucl. Phys. **A837** (2010) 26.
[23] T. Hirano and K. Tsuda, Phys. Rev. C **66** (2002) 054905; P. F. Kolb and R. Rapp, Phys. Rev. C **67** (2003) 044903; P. Huovinen, Eur. Phys. J. **A37** (2008) 121.
[24] P. Braun-Munzinger, D. Magestro, K. Redlich and J. Stachel, Phys. Lett. **B518** (2001) 41; J. Adams *et al.* [STAR Collaboration], Nucl. Phys. **A757** (2005) 102; A. Andronic, P. Braun-Munzinger and J. Stachel, Phys. Lett. **B673** (2009) 142 [Erratum-ibid. **B678** (2009) 516].
[25] D. Kharzeev and M. Nardi, Phys. Lett. **B507** (2001) 121;

D. Kharzeev, E. Levin and M. Nardi, Nucl. Phys. **A730** (2004) 448 [Erratum-ibid. **A743** (2004) 329].
[26] A. Adil, H. J. Drescher, A. Dumitru, A. Hayashigaki and Y. Nara, Phys. Rev. C **74** (2006) 044905; H. J. Drescher and Y. Nara, Phys. Rev. C **75** (2007) 034905.
[27] C. E. Aguiar, Y. Hama, T. Kodama and T. Osada, Nucl. Phys. **A698** (2002) 639; O. . J. Socolowski, F. Grassi, Y. Hama and T. Kodama, Phys. Rev. Lett. **93** (2004) 182301; R. Andrade, F. Grassi, Y. Hama, T. Kodama and O. J. Socolowski, Phys. Rev. Lett. **97** (2006) 202302.
[28] H. Holopainen, H. Niemi and K. J. Eskola, arXiv:1007.0368 [hep-ph].
[29] H. Petersen, G. Y. Qin, S. A. Bass and B. Müller, arXiv:1008.0625 [nucl-th].
[30] B. Schenke, S. Jeon and C. Gale, arXiv:1009.3244 [hep-ph].
[31] E. Schnedermann, J. Sollfrank and U. Heinz, NATO Adv. Study Inst. Ser. B Phys. **303** (1993) 175; and Phys. Rev. C **48** (1993) 2462.
[32] S. A. Bass and A. Dumitru, Phys. Rev. C **61** (2000) 064909.
[33] T. Hirano, U. Heinz, D. Kharzeev, R. Lacey and Y. Nara, Phys. Lett. **B636** (2006) 299.
[34] T. Hirano and M. Gyulassy, Nucl. Phys. **A769** (2006) 71.
[35] P. Romatschke and U. Romatschke, Phys. Rev. Lett. **99** (2007) 172301.
[36] K. Dusling and D. Teaney, Phys. Rev. C **77** (2008) 034905.
[37] M. Luzum and P. Romatschke, Phys. Rev. C **78** (2008) 034915 [Erratum-ibid. C **79** (2009) 039903].
[38] U. Heinz, J. S. Moreland and H. Song, Phys. Rev. C **80** (2009) 061901.
[39] S. S. Adler *et al.* [PHENIX Collaboration], Phys. Rev. C **69** (2004) 034909.
[40] A. Adare *et al.* [PHENIX Collaboration], Phys. Rev. Lett. **98** (2007) 162301.
[41] C. A. Salgado and U. A. Wiedemann, Phys. Rev. D **68** (2003) 014008.
[42] S. Caron-Huot and C. Gale, 1006.2379 [hep-ph].
[43] K. Zapp, J. Stachel and U. A. Wiedemann, Phys. Rev. Lett. **103** (2009) 152302.
[44] T. Renk, 1010.4116 [hep-ph].
[45] C. Marquet and T. Renk, Phys. Lett. **B685** (2010) 270.
[46] S. S. Gubser, D. R. Gulotta, S. S. Pufu and F. D. Rocha, JHEP **0810**, 052 (2008); P. M. Chesler, K. Jensen, A. Karch and L. G. Yaffe, Phys. Rev. D **79**, 125015 (2009).
[47] T. Renk, Phys. Rev. C **76** (2007) 064905.
[48] J. Auvinen, K. J. Eskola, H. Holopainen and T. Renk, arXiv:1008.4657 [hep-ph].
[49] C. A. Salgado and U. A. Wiedemann, Phys. Rev. Lett. **89** (2002) 092303.
[50] R. Baier, A. H. Mueller and D. Schiff, Phys. Lett. **B649** (2007) 147.
[51] H. Liu, K. Rajagopal and U. A. Wiedemann, JHEP **0703** (2007) 066.
[52] T. Renk and K. Eskola, Phys. Rev. C **75** (2007) 054910.
[53] B. A. Kniehl, G. Kramer and B. Potter, Nucl. Phys. **B582**, 514 (2000).
[54] T. Renk, Phys. Rev. C **78** (2008) 034904
[55] J. Pumplin, D. R. Stump, J. Huston, H. L. Lai, P. Nadolsky and W. K. Tung, JHEP **0207** (2002) 012.
[56] D. Stump, J. Huston, J. Pumplin, W. K. Tung, H. L. Lai, S. Kuhlmann and J. F. Owens, JHEP **0310** (2003) 046.
[57] M. Hirai, S. Kumano and T. H. Nagai, Phys. Rev. C **70** (2004) 044905.
[58] K. J. Eskola, V. J. Kolhinen and C. A. Salgado, Eur. Phys. J. **C9** (1999) 61.
[59] G. Corcella *et al.*, JHEP **0101** (2001) 010. hep-ph/0210213.
[60] T. Renk and J. Ruppert, Phys. Rev. C **73** (2006) 011901.
[61] S. Afanasiev *et al.* [PHENIX Collaboration], Phys. Rev. C **80** (2009) 054907.
[62] J. Liao and E. Shuryak, Phys. Rev. Lett. **102** (2009) 202302.
[63] G. Policastro, D. T. Son and A. O. Starinets, Phys. Rev. Lett. **87** (2001) 081601; P. Kovtun, D. T. Son and A. O. Starinets, Phys. Rev. Lett. **94** (2005) 111601.